Chemical Senses, 2015, 1–10
doi:10.1093/chemse/bjv018
Original Article

Original Article

Characterization of Sensory Properties of Flavanols—A Molecular Dynamic Approach

Raúl Ferrer-Gallego[1,2], Natalia Quijada-Morín[1], Natércia F. Brás[3], Paula Gomes[3], Victor de Freitas[2], Julián C. Rivas-Gonzalo[1] and M. Teresa Escribano-Bailón[1]

[1]Grupo de Investigación en Polifenoles, Unidad de Nutrición y Bromatología, Facultad de Farmacia, Universidad de Salamanca, Campus Miguel de Unamuno, E 37007 Salamanca, Spain, [2]REQUIMTE/LAQV, Departamento de Química e Bioquímica, Faculdade de Ciências, Universidade do Porto, Rua do Campo Alegre, 4169-007 Porto, Portugal and [3]REQUIMTE/UCIBIO, Departamento de Química e Bioquímica, Faculdade de Ciências, Universidade do Porto, Rua do Campo Alegre, s/n, 4169-007 Porto, Portugal

Correspondence to be sent to: M. Teresa Escribano-Bailón, Grupo de Investigación en Polifenoles. Unidad de Nutrición y Bromatología, Facultad de Farmacia, Universidad de Salamanca, Campus Miguel de Unamuno, E 37007 Salamanca, Spain. e-mail: escriban@usal.es

Abstract

In this work, sensations elicited by catechin and procyanidins in comparison with those elicited by gallocatechin and prodelphinidins were evaluated by means of a sensory panel. To obtain further insights into the mechanisms of action, molecular dynamics (MD) simulations and saturation transfer difference nuclear magnetic resonance (STD NMR) experiments have been performed. Results showed clear differences between the 2 types of flavanols. Dihydroxylated B-ring flavanols were more astringent, bitter, dry, rough, unripe, and persistent than trihydroxylated B-ring ones. Besides, these last compounds were smoother, more velvety, and viscous. MD simulations and STD NMR experiments support results obtained from tasting panel. MD results suggested that catechin binds to a human salivary proline-rich peptide $IB7_{14}$ faster than gallocatechin and this interaction is maintained longer. $IB7_{14}$ can interact with 2 catechin molecules concurrently while only interacts with 1 gallocatechin molecule. Accordingly, STD NMR experiments showed a greater affinity of catechin than gallocatechin for the peptide (K_D = 2.7 and 25.7, respectively). Results indicate that the number of hydroxyl substituents present in B-ring of the flavanic nucleus is decisive for the interaction with salivary proteins and the development of astringency perception.

Key words: astringency, bitterness, flavanols, IB7, molecular dynamic simulations, STD NMR

Introduction

Tannins are a large and complex group of polyphenolic compounds commonly found in plants, food, and beverages. Generally, these compounds are divided in 2 major classes: condensed and hydrolyzable tannins. The first ones or proanthocyanidins, are structurally divided in procyanidins (polymers of catechin [CAT]) and prodelphinidins (polymers of gallocatechin [GAL]).

Several tannins have the ability to precipitate proteins, which is related to the development of the astringency sensation in the oral cavity (Soares et al. 2012). In grapes, they are mainly located in seeds and skins and they are transferred into the wine during the maceration-fermentation process. Although procyanidins are commonly found in both parts of the berry, prodelphinidins are exclusively located in skins. The amount of prodelphinidins is higher when the climate conditions are propitious for a good maturity indicating a greater potential to elaborate high quality red wines (Ferrer-Gallego et al. 2012a; Gil et al. 2012). It is well known that procyanidins contribute directly to the astringency (Ferrer-Gallego et al. 2010),

nonetheless the contribution of prodelphinidins on the sensory perception has not been well established.

Astringency is one of the most important sensory attributes of food and beverages. This attribute is a complex sensation that implies multiple mechanisms and that can be accompanied simultaneously by other tastes or mouth-feel characteristics (Lee and Lawless 1991; Rossetti et al. 2009; Gibbins and Carpenter 2013). It is well accepted that astringency involves different oral sensations, including drying, puckering, shrinking, drawing, harshness, and roughness among other attributes (Gawel et al. 2001). Tannins may elicit many of these mouth-feel characteristics but the relation structure-oral sensation remains to be established.

Interaction between tannins and proteins is recognized as the main mechanism in astringency development (de Freitas and Mateus 2012; Scollary et al. 2012). Nevertheless, controversies between sensory studies and tannin-protein interaction have been shown in literature, (Ferrer-Gallego et al. 2012b; Lee et al. 2012). Protein precipitation seems to be not the only mechanism in the astringency perception. In this way, Gibbins and Carpenter (2013) have recently proposed possible mechanisms of astringency occurring simultaneously in the oral cavity, such as alterations on salivary film and pellicle, changes in rheological and lubricating properties of the salivary film, and the activation of transient receptor protein channel (Kurogi et al. 2012) or laminin receptor (Schwarz and Hofmann 2008).

Recent works have been focused on the implication of wine tannins structure on their sensory properties. Some authors have postulated that the mean degree of polymerization of tannins does not have a significant influence on the astringency perception (Wollmann and Hofmann 2013). In contrast, it has been suggested that polymeric procyanidins (degree of polymerization from 12 to 34) show higher astringency intensity than the oligomeric ones (from 2 to 15) (Sun et al. 2013). Recently, it has been stated that the larger tannins of wine, which are more water soluble, are more astringent than the smaller ones, which are perceived as more bitter (McRae et al. 2013). Bitterness and astringency of the smallest flavanols have also been evaluated showing (−)-epicatechin more bitter and more astringent than (+)-catechin (Ferrer-Gallego et al. 2014). This fact proves the effect of the stereochemistry of flavan-3-ols on the sensory perception (Thorngate and Noble 1995; Kallithraka et al. 1997). Despite several studies were made in order to study the sensory profile of phenolic compounds, none of them included prodelphinidins.

In this work, the sensory profile of monomers, dimers and trimers of proanthocyanidins have been characterized by a sensory panel. The relationships of these profiles and the proanthocyanidin structures have been described and results obtained have been explained by means of molecular dynamics simulations and saturation-transfer difference (STD) NMR. For this purpose, the conformational behavior of CAT and GAL with a fragment of the peptide IB7, which contains a characteristic sequence of proline rich proteins, has been characterized.

Materials and methods

Chemicals

All solvents were of HPLC grade and all chemicals were of analytical reagent grade. Ultrapure water was obtained from a Milli-Q Gradient water purification system (Millipore). Deuterium oxide (99.9%), (+)-CAT (C) and (−)-GAL (GC) standards were supplied by Sigma–Aldrich.

Isolation of proanthocyanidin dimers and trimers

Proanthocyanidins dimers and trimers were obtained from barley. This source was selected due to the high content of prodelphinidins reported in bibliography (Madigan et al. 1994). Extraction was performed using acetone-water (3:1). Acetone was removed and n-hexan was used to eliminate lipophilic material in the extract. The aqueous solution was filtered through 0.45 µm filters before proanthocyanidin isolation by semi-preparative HPLC-DAD.

Preparative separation was performed in an Agilent 1260 Infinity series Preparative LC. (Agilent Technologies) consisting of a thermostated autosampler, 2 coupled preparative pumps which formed a binary system, a diode array detector and a thermostated sampler collector, controlled by OpenLab CDS Chemstation Workstation software (version C.01.04; Agilent Technologies). UV-Vis spectra were recorded from 200 to 600 nm, while acquiring at the preferred wavelength 280 nm.

Chromatographic separations of proanthocyanidins were performed in 2 successive steps. For the first step, a reverse phase Agilent Prep C18 (50 mm × 150 mm × 10 µm) was used. Mobile phases A and B were respectively acetic acid 2.5% in water and HPLC grade methanol. The elution profile was as follows: hold and isocratic flow at 0% B for 1 min, from 0% to 6% B for 2 min, from 6% to 20% B for 33 min, from 20% to 50% B for 7 min, from 50% to 75% B for 6 min, from 75% to 100% B for 2 min and from 100% to 0% B for 5 min. The flow-rate was 25 mL/min and the injection volume was 45 mL.

Procyanidin rich fraction was submitted to a second separation using a reverse phase Agilent Prep C18 (21.2 mm × 150 mm × 5 µm). The flow rate was set at 15 mL/min and the injection volume was 5 mL. Mobile phases A and B were respectively acetic acid 2.5% in water and HPLC grade methanol, the gradient program was as follows: from 0% to 15% B for 25 min, from 15% to 30% B for 5 min, from 30% to 50% B for 2 min, from 50% to 75% B for 3 min, from 75% to 100% B for 2 min and from 100% to 0% in 3 min. Procyanidin dimer B3 (dimer of CATs) and procyanidin trimer C2 (trimer of CATs) were isolated form this fraction. Prodelphinidin rich fraction was submitted to a second purification using a reverse phase Agilent Prep C18 (21.2 mm × 150 mm × 5 µm); the flow rate was 18 mL/min and the injection volume was 5 mL. The elution conditions were as follows: from 0% to 7% B for 1 min, from 7% to 7.8% B for 11 min, from 7.8% to 10% B for 2 min, from 10% to 50% B for 2 min, from 50% to 75% B for 2 min, and from 75% to 0% B for 2 min. A mixture of dimers containing GAL and CAT subunits and a mixture of trimers containing CAT as terminal unit and GAL and CAT as extension units were isolated from this fraction.

Characterization of the compounds was performed by acid cleavage.

Identification of the isolated compounds

Acid catalyzed cleavage of proanthocyanidins was performed in presence of phloroglucinol to characterize the isolated compounds, following the procedure described by Kennedy and Jones (2001) with minor modifications, as follows: a solution containing 0.2 M HCl, 50 mg/mL phloroglucinol and 10 mg/mL l-ascorbic acid was prepared in methanol as phloroglucinolysis reagent. One milligram of each isolated compound was solved in 100 µL methanol and allowed to react with 200 µL phloroglucinol solution in a pre-heated water bath at 50 °C for 40 min. Afterwards, the reaction was cooled down and quenched by the addition of 2.7 mL of 15 mM sodium acetate aqueous solution. The reaction mixture was then purified by SPE and analyzed by HPLC–DAD–ESI/MS following the procedure described elsewhere (Quijada-Morin et al. 2012).

Sensory analysis

The trained sensory panel was composed by 10 wine-taster experts, 3 women and 7 men, aged from 29 to 60 years old. The panel was

made up by 4 professors of sensory analysis and oenology of the Polytechnic University of Valencia; 2 professional wine-tasters and members of national and international wine tasting juries; 2 oenologists and 2 final year students of oenology. Tasters were volunteers, not paid and not informed about the identity of the samples.

All the panellists were previously trained although they already had experience in tasting phenolic compounds. The panel had participated in recent experiences carried out by our research group, and reliability of the panel was proved (Ferrer-Gallego et al. 2014).

The training samples consisting in aqueous solutions of quinine hydrochloride dihydrate (0.025–0.1 g/L) to carry out the assays of bitterness, aluminium potassium sulphate (0.25–1 g/L) and tannic acid (0.175–1.5 g/L) for astringency, tartaric acid (0.125–1 g/L) for sourness, glucose (1–10 g/L) for sweet, NaCl (0.25–1 g/L) for salty, sodium l-glutamate 1-hydrate (0.25–1 g/L) for the umami, glycerol (5–20 g/L) and aqueous gelatine solutions (0.25–0.5%) for smoothness and viscosity.

In the training sessions tasters also became familiar with intensity rating using a Labelled Magnitude Scale (LMS) (Green et al. 1996). This is a useful tool to measuring the perceived intensity of sensory attributes consisting in a semantic scale by a quasi-logarithmic space from 0 to 100 (barely detectable ~2; weak ~7; moderate ~16; strong ~34; very strong ~50; strongest imaginable ~100).

The sensory attributes evaluated were: intensity of astringency, bitterness, drying, roughness, unripe (greenness), smoothness, velvety, viscosity, and persistence.

Proanthocyanidins compounds: GAL, dimers and trimers of prodelphinidins, CAT, dimer B3, and trimer C2 were dissolved separately in mineral water at pH 3.6 at concentration 1.5 g/L. These phenolic compounds showed a moderate feeling at this concentration allowing an upper and lower perception. Similar concentrations have been used in order to evaluate bitterness and astringency of CATs (Robichaud and Noble 1990; Kallithraka et al. 1997). Tasters placed 5 mL of the solution in the mouth, swilled it around for 15 s, spitted the samples out and then rated the attributes in the LMS. The attribute persistence was rated 2 min after the sample was expectorated.

Optimization and molecular dynamics simulations

Two virtual systems containing a peptide model $IB7_{14}$ and either CAT or GAL molecules were built. Since human salivary proline-rich proteins (PRPs) belong to the natively unfolded protein family and their structures show repeated domains (as $IB7_{14}$) without any stable tertiary structure, the shorter representative—the $IB7_{14}$ peptide—was specifically chosen to understand at an atomistic level the different steps that govern the recognition process between PRPs and CAT or GAL molecules. Similar procedures were successfully employed by Cala et al. (2010, 2011, 2012) to study the association of tannins to salivary proteins. The GaussView software (Gaussian, Inc.) was used to create both phenolic structures, which were further optimized with the HF/6-31G(d) level of theory and using the Gaussian 09 suite of programs (Frisch et al. 2009). The RESP algorithm (Bayly et al. 1993) was used to recalculate the atomic charges. The previous calculations were used for the parameterization of these molecules using the antechamber tool. The force fields GAFF (Wang et al. 2004) and parm99 (Cornell et al. 1995) were used to characterize the phenolic compounds and the peptide, respectively, during the geometry optimization and molecular dynamics (MD) simulations. An explicit solvation model with pre-equilibrated TIP3P water molecules was used, filling a truncated rectangular box with a minimum distance of 20 Å between the box faces and any atom of each system. Eight phenolic molecules were randomly positioned near the $IB7_{14}$ fragment of each system to reproduce the conditions used in the experimental sensory analysis (flavan-3-ol concentration = 1.5 g/L). To release the bad contacts in the structures, the system geometries were minimized in 2 stages. MD simulations of 100 ps at NVT ensemble, and considering periodic boundaries conditions were run, followed by 40 ns of MD simulation with an isothermal-isobaric NPT ensemble (constant number of particles, pressure, and temperature). The temperature was maintained at 303.15 K (Izaguirre et al. 2001) using a Langevin dynamics thermostat (collision frequency of 1.0/ps). Both MD simulations were performed using the AMBER 12.0 simulations package (Case et al. 2012). The SHAKE and the Verlet leapfrog algorithms were used to constrain the hydrogen bonds, and to integrate the equations of motion with a time step of 2 fs (Ryckaert et al. 1977). A cutoff of 10 Å was used to truncate the nonbonded interactions, while the Particle-Mesh Ewald method (Essmann et al. 1995) was employed to include long-range interactions. The simulations involving both $IB7_{14}$:$(CAT)_8$ and $IB7_{14}$:$(GAL)_8$ were repeated 3 times starting from different initial velocities and geometries. This was performed in order to increase the sampling and evaluate different paths of the systems. Furthermore, an additional MD simulation (60 ns) was performed with only 1 molecule of CAT (or GAL) (instead of 8 molecules) and 1 molecule of $IB7_{14}$. This latter experiment was used to confirm the specificity of the interaction flavanol-peptide and to avoid the self-association of polyphenols. The analysis of the MD trajectories was carried out with the PTRAJ module of AMBER 12.0 (Case et al. 2012). A similar protocol using MD simulations was recently applied to study the interactions between carbohydrates and anthocyanin molecules (Fernandes et al. 2014).

STD NMR experiments

Taking advantage of having peptide $IB7_{12}$ already available at our lab, which only lacks the N-terminal Ser-Pro residues compared with $IB7_{14}$, we sought for experimental confirmation of computational evidences. Hence, the peptide $IB7_{12}$ (PGKPQGPPPQGG [C-terminal amide]) was used for the STD NMR analysis which was assembled by Fmoc/tBu solid-phase peptide synthesis methodologies (Fields and Noble 1990; Collins and Leadbeater 2007). Conveniently protected amino acids were sequentially coupled in the C→N direction. The Fmoc deprotection step was carried out using 20% piperidine in DMF (dimethylformamide). The coupling step was performed using 5 molar equivalents (eq) of the Fmoc-protected amino acid in DCM (dichloromethane) (0.2 M) and 5 eq of DIPCI (diisopropylcarbodiimide) and carried out for 1 h. Once the peptide chain was assembled, acidolytic cleavage of peptide-resin support was carried out by standard methods using a trifluoroacetic acid (TFA)-based cocktail containing triisopropysilane (TIS) as scavenger (TFA/DCM/TIS 70:25:5 v/v/v) (Fields 1997). Crude product was purified by reverse-phase liquid chromatography to give the target peptide, as confirmed by HPLC (Hitachi-Merck LaChrom Elite), LC-ESI/IT MS (LCQ-DecaXP LC-MS system, ThermoFinnigan) and UV spectrometry. Peptide quantification was performed by amino acids analysis.

A 0.5 mM of the peptide solution was prepared in D_2O and transferred into 5 mm NMR tube in order to keep the peptide concentration constant throughout the STD experiments. GAL and CAT solutions were lyophilized and added (from 1 to 9 mM) to the peptide solution.

STD effect was determined using the amplification factor (A_{STD}) according to the following equation (Viegas et al. 2011).

$$A_{STD} = \frac{I_0 - I_{SAT}}{I_0} \cdot x \cdot \frac{[T]}{[P]} = \frac{I_{STD}}{I_0} \cdot x \cdot \frac{[T]}{[P]} \quad (1)$$

where I_{SAT} is the signal intensity of the selectively saturated protein spectrum (*on-resonance*) and I_0 is the signal intensity of the spectrum recorded without protein saturation (*off-resonance*). [T] is the tannin concentration and [P] is the peptide concentration. The determination of the dissociation constant (K_D) was calculated according to the equation (2).

$$A_{STD} = \frac{\alpha_{STD} + [T]}{K_D + [T]} \quad (2)$$

where α_{STD} is the maximum amplification factor. For the K_D determination nonlinear least-squares-fitting curve by Solver tool of Microsoft Excel was used.

NMR experiments were recorded on a Bruker Avance III 400 MHz spectrometer, equipped with a 5 mm PABBI 1H/D-BB and pulse gradient units capable of producing magnetic field pulsed gradients in the z direction of 50 G/cm. The measurements were made with standard Bruker pulse sequences at 26 °C. 1H and STD spectra were recorded with a shaped pulse to suppress the water resonance using the following parameters: spectral width, 16 ppm; nutation angle, 7.8 μs and 90°; and shaped pulse duration, 2 ms. Selective saturation of the peptide *off*-resonance at 16 ppm and *on*-resonance at −0.5 ppm was performed using a pseudo-two-dimensional (2D) sequence for STD with a shaped pulse train alternating between the *on* and *off* resonances (Gonçalves et al. 2011). STD-NMR spectra were acquired using Gaus 1.1000 pulses for selective saturation (50 ms), with a total saturation time of 2.5 s. The number of scans (16), receptor gain value (114), and relaxation delay (3.5 s) were kept constants. To subtract the unprocessed on and off-resonance spectra, to baseline correct the resulting difference spectrum and to integrate the areas, TopSpin 2.1 software from Bruker was used.

Statistical treatment

Principal components analysis (PCA), an unsupervised pattern recognition method, was used for data analysis. The IBM SPSS 21 for Windows software package (SPSS, Inc.) was used for data processing.

Ethics statement

This study complies with the policies laid down by the Helsinki declaration and had been approved by the Bioethics Committee of the University of Salamanca. All the tasters were informed about the aim of the research and all of them expressed their consent to participate in this study.

Results and discussion

Sensory analysis

Table 1 shows the results obtained in the sensory analysis. For each attribute, results are presented according to the percentage of the panellists that consider the sensation elicited by the compound in the first column lower, equal or higher than the sensation elicited by the compound in row.

Comparison between trihydroxylated B-ring and dihydroxylated B-ring flavanols shows that tasters considered GAL less astringent, bitter, dry, rough unripe, and persistent than CAT. On the contrary, GAL presented higher smoothness, velvety, and viscosity. Comparing proanthocyanidins, tasters stated that prodelphinidin trimers (PDT) were less astringent, bitter, dry, rough, unripe, and persistent than procyanidin trimers (PCT). However, they presented higher smoothness, velvety, and viscosity. Similarly, prodelphinidin dimers (PDD) were less astringent, bitter, dry, rough, unripe and persistent than procyanidin dimers (PCD), although they presented higher velvety and viscosity. Similar behavior can be obtained from the comparison between prodelphinidins (dimers and trimers) and the monomer CAT. That is to say, PDT and PDD were less astringent, bitter, dry, rough, and unripe than CAT, but they presented higher smoothness, velvety, and viscosity. These observations suggest that the number of hydroxyl substituents (2 in procyanidins, and 3 in prodelphinidins) in the B ring of the proanthocyanidins structure determine the quality of the astringency perception. Positive sensory attributes (smoothness, velvety, and viscosity) are more intense in trihydroxylated than in dihydroxylated proanthocyanidins, which are more related to negative attributes (i.e., bitter, rough, and unripe). This reinforces the idea that high amounts of trihydroxylated B-ring in grapes could be related to a greater potential to elaborate high quality red wines (Gil et al. 2012).

On the other hand, the fact that procyanidins seemed to be more persistent than prodelphinidins could indicate that the unpleasant sensations linked to procyanidins were more persistent than the sensations linked to prodelphinidins.

Regarding the number of units of the flavanol, from monomers to trimers, it can be observed that higher number of flavanol units in the molecule is related with less intensity of negative sensory attributes and more intensity of positive attributes. Hence proanthocyanidins are more related to smoothness or velvety than monomers. This is more noticeable between trimers and monomers than between dimers and monomers, and also than between trimers and dimers. In particular, PDT elicited a sensation less astringent, bitter, dry, rough, and unripe than the GAL, but more smooth and viscose. In turn, PCT elicited a sensation less astringent, bitter, dry, and rough than the CAT, but more persistent and velvety. Hence, the number of subunits constituting the flavanol seems to have noticeable influence in the bitterness and in the intensity and qualitative characteristics of the astringency elicited in mouth.

In order to better explain relationships between the attributes and the phenolic compounds, a principal component analysis (PCA) was carried out. The data matrix was constituted by the sensory scores. Figure 1 shows the score plot and the loading plot defined by the first and second principal components. The first principal component (PC1) describes 91.4% of the variability in the data and the second component (PC2) describes 4.1%. In the score plot, the procyanidins (CAT, PCD, and PCT) presented negatives scores in PC1, showing CAT the most negative value. On the contrary, prodelphinidins (GAL, PDD, and PDT) presented positive values in this principal component, showing PDT the most positive value. In this plot, it can also be seen that PCT and PCD presented similar scores in this PC as occurred in the case of GAL and PDD.

In the loading plot, it can be observed that variables considered as positive oral attributes (velvety, smoothness, and viscosity) presented positive scores in PC1. On the other hand, variables considered as negative sensations presented negative scores. The most important variables in PC1 were intensity of astringency and velvety. This pattern suggests that procyanidins are more related with unpleasant oral sensations (intensity of astringency, bitterness, unripe, harsh, and drying) whereas prodelphinidins are linked to good oral sensations.

Among prodelphinidins, it seems that trimers (PDT) were more associated with good sensations than dimers and gallocatechin. In this way, CAT was more related with bad sensations that procyanidin dimers and trimers, primarily with bitterness perception.

Persistence seems to be more related with the unpleasant sensations (procyanidins) than with the agreeable ones (prodelphinidins).

Table 1. Percentage of panelist that consider the sensation elicited by compound in the first column lower (<), equal (=), or higher (>) than the sensation elicited by compound in row

	PDD			GAL			PCT			PCD			CAT		
	<	=	>	<	=	>	<	=	>	<	=	>	<	=	>
Astringency, %															
PDT	50	50	0	60	0	40	90	0	10	80	10	10	90	0	10
PDD				50	0	50	90	0	10	80	10	10	90	0	10
GAL							70	20	10	70	20	10	80	20	0
PCT										50	20	30	80	0	20
PCD													80	0	20
Bitterness, %															
PDT	50	30	20	70	10	20	70	20	10	70	30	0	90	0	10
PDD				60	10	30	60	10	30	60	20	20	100	0	0
GAL							60	10	30	50	30	20	100	0	0
PCT										60	10	30	90	10	0
PCD													90	10	0
Drying, %															
PDT	70	0	30	60	10	30	100	0	0	90	10	0	100	0	0
PDD				40	20	40	60	20	20	70	0	30	60	10	30
GAL							70	10	20	80	0	20	80	0	20
PCT										80	0	20	70	0	30
PCD													30	50	20
Roughness, %															
PDT	70	0	30	80	0	20	80	10	10	100	0	0	90	10	0
PDD				30	20	50	80	20	0	70	10	20	80	0	20
GAL							90	10	0	80	0	20	80	0	20
PCT										50	10	40	60	10	30
PCD													60	20	20
Unripe, %															
PDT	60	20	20	60	10	30	80	10	10	80	20	0	90	0	10
PDD				30	50	20	70	10	20	70	20	10	90	0	10
GAL							90	0	10	90	0	10	90	10	0
PCT										40	30	30	40	30	30
PCD													50	40	10
Persistence, %															
PDT	30	10	60	50	20	30	70	10	20	80	0	20	60	10	30
PDD				60	10	30	90	0	10	70	30	0	50	20	30
GAL							80	10	10	70	20	10	50	30	20
PCT										20	40	40	20	20	60
PCD													30	30	40
Smoothness, %															
PDT	20	50	30	10	30	60	10	10	80	0	10	90	0	20	80
PDD				40	20	40	40	10	50	50	10	40	30	10	60
GAL							10	30	60	0	30	70	10	10	80
PCT										10	50	40	20	30	50
PCD													20	60	20
Velvety, %															
PDT	30	10	60	20	30	50	0	0	100	10	0	90	0	0	100
PDD				50	0	50	10	0	90	30	10	60	10	0	90
GAL							10	0	90	10	0	90	0	10	90
PCT										20	20	60	30	10	60
PCD													20	20	60
Viscosity, %															
PDT	30	0	70	30	0	70	20	0	80	10	0	90	20	0	80
PDD				30	0	70	10	30	60	20	10	70	30	10	60
GAL							30	0	70	0	40	60	20	20	60
PCT										20	30	50	50	20	30
PCD													30	50	20

Molecular dynamics simulations

To better characterize the conformational behavior of CAT and GAL molecules with the peptide fragment $IB7_{14}$ in aqueous solution, computational studies were additionally carried out. Two MD simulations ($IB7_{14}$:CAT and $IB7_{14}$:GAL model systems) were carried out to evaluate the specificity of the interaction and avoid any self-association of polyphenols. Considering the CAT containing model, the interaction occurs at 45 ns; whereas for the model involving gallocatechin, the interaction was observed at 42 ns. In both models, the CAT/gallocatechin molecules remain bound to the $IB7_{14}$ peptide

for the rest of the simulation, which points to the higher stability of these interactions. Furthermore, another 6 MD simulations of 40 ns each were performed [3 with $IB7_{14}$:$(CAT)_8$ and 3 with $IB7_{14}$:$(GAL)_8$ model systems]. In all the simulations, and after the first nanosecond, the root-mean-square deviation (RMSD) values of the $IB7_{14}$ backbone stabilizes. This supports the overall stability and equilibration of the peptide structures. In general, the MD simulations performed show the formation of stable complexes, involving polyphenol molecules and residues of the proline-rich protein fragment (Figure 2). Table 2 summarizes for each MD setting, different time indicators considering the formation of both peptide-CAT and peptide-GAL complexes.

It was observed that the first interaction between a phenolic group and the peptide took place more quickly in the systems with 8 polyphenols than with a single CAT/GAL molecule. In addition, the formation of the peptide–polyphenol complex is faster considering CAT, than gallocatechin. The total time they remained bound and the maximum uninterrupted binding time, obtained for 1 and 2 molecules, are also higher for the peptide-CAT simulations. Analyzing the MD-1 simulation, after only 3.8 and 6.6 ns, one and a second CAT molecule (respectively) bounded to the peptide. This structural arrangement—25% of the CAT molecules bound to the $IB7_{14}$ peptide—was maintained throughout 20.2 ns of simulation, revealing its higher stability. A similar behavior has been previously proposed for proanthocyanidin B3 (Simon et al. 2003), in which the cooperative linkage of molecules to the same peptide was also observed. However, the analysis of the MD-1 simulation with GAL molecules reveals that the maximum binding was achieved later—at 9.3 ns—and for only of one molecule. This first molecule ceased to interact with the peptide after a few picoseconds and only at 20 ns of simulation another molecule of gallocatechin was bound to $IB7_{14}$. This structural arrangement with 12.5% of binding (only 1 gallocatechin) was maintained throughout 16.8 ns, being the maximum uninterrupted binding of only 4.8 ns. In general, the behavior of the 3 simulations of each system is similar between them, which validate these results. In summary, all MD simulations revealed that both polyphenols interact with the peptide, but the binding of gallocatechin molecules to $IB7_{14}$, was weaker than the one observed for the $IB7_{14}$:$(CAT)_8$ system.

Figure 2 shows representative structures of both peptide-CAT and peptide-GAL complexes, in which the main binding driving forces (hydrophobic contacts and hydrogen-bonds [H-bonds]) were identified. Figure 2A depicts some H-bonds established between the hydroxyl groups of CAT molecules and the backbone carbonyl groups of the peptide molecule. The short length of the exemplified H-bonds reinforces the strong binding of these compounds to the peptide. The involvement of hydrophilic bonds as the main driving force in the interaction tannin-protein has already been suggested (de Freitas et al. 2003; Simon et al. 2003). In our study, it was also observed that the peptide tends to adopt a semi-coiled structure, in which 2 CAT molecules are strongly encapsulated by the formation of many hydrophobic and hydrophilic interactions. In this particular

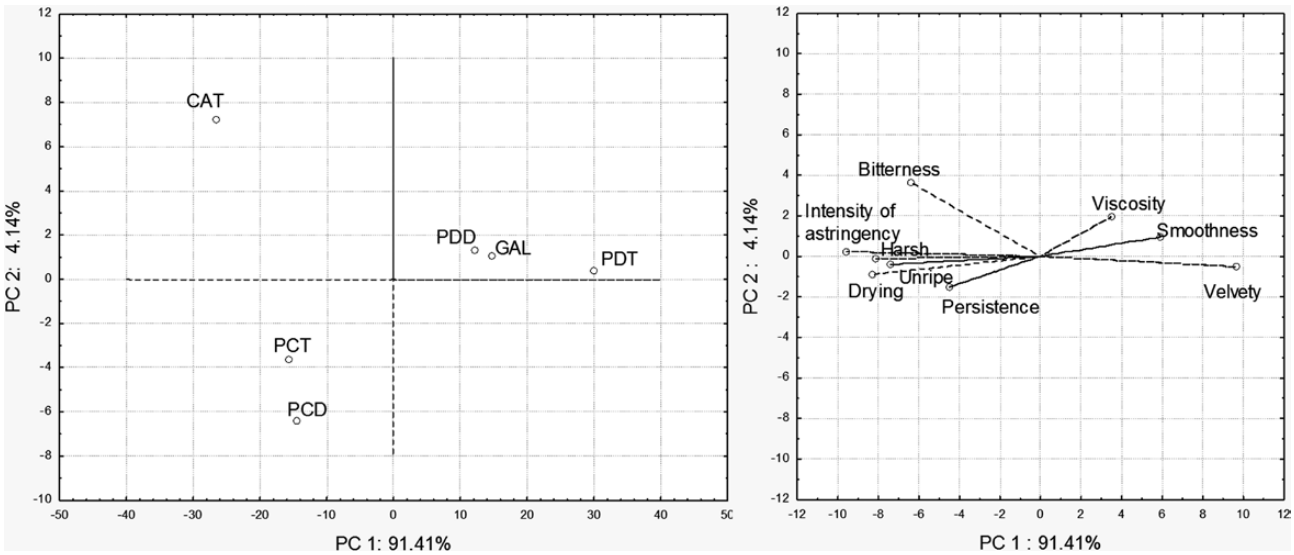

Figure 1. Principal component analysis of the sensory attributes of the phenolic compounds. CAT, catechin; GAL, gallocatechin; PCD, procyanidin dimers; PDD, prodelphinidin dimer; PCT, procyanidin trimers, and PDT, prodelphinidin trimers.

Table 2. The binding of polyphenols (CAT and GAL) to the $IB7_{14}$ peptide was analyzed by: 1. time of binding; 2. total time it remained bound; and 3. the maximum uninterrupted binding time

	$IB7_{14}$:$(catechin)_8$			$IB7_{14}$:$(gallocatechin)_8$		
	MD-1	MD-2	MD-3	MD-1	MD-2	MD-3
Time of binding of the 1st polyphenol/ns	3.8	1.7	6.3	9.3	34.7	4.1
Time of binding of 2 polyphenols (simultaneously)/ns	6.6	—	—	—	37	39.5
Total binding time of 1 polyphenol/ns	16	15.7	24.4	16.8	4.4	21.2
Total binding time of 2 polyphenols/ns	20.2	—	—	—	0.9	0.5
Maximum uninterrupted binding time of 1 polyphenol/ns	3.8	14.7	19.1	4.8	3.2	14.5
Maximum uninterrupted binding time of 2 polyphenols/ns	20.2	—	—	—	0.9	0.5

structure, 1 CAT molecule establishes H-bonds with the carbonyl groups of Pro2, Gln7, and Gly8, as well as it made hydrophobic contacts with the Pro2, Pro6, and Pro11 residues. The second CAT unit has H-bridges with the Ser1 and Pro9 residues (side chain and carbonyl backbone groups, respectively), and establishes dispersive contacts with Pro10 and Pro11. Interestingly, the GAL molecule interacts with the extended structure of the peptide, mainly by hydrophilic interactions with Gln7 and Gly8 residues, and some hydrophobic contacts with Pro6, Pro9, and Pro10 residues (Figure 2B). The conformational change of the peptide fragment from an extended conformation to a more compact one has been described as a part of the first step of the model currently accepted for the interaction between tannins and proline-rich proteins (Jobstl et al. 2004).

When comparing both polyphenols, it can be said that CAT molecules interact more with the $IB7_{14}$ peptide than GAL units. However, in the $IB7_{14}$:$(GAL)_8$ simulations, it was detected the occurrence of some assemblies of 2 GAL molecules that are perfectly aligned between themselves by their surfaces. Since GAL molecules interact with each other and form clusters between them, the phenolic area exposed for the peptide interaction is smaller and this could be responsible for the weak interaction observed with the peptide. Previous observations on other proanthocyanidin compounds suggested that the more the phenolic parts are exposed, the greater the affinity for the peptide (Cala et al. 2010). On the other hand, the representative theoretical structures of the flavanol–peptide complexes (Figure 2) show an extended conformation for gallocatechin–peptide interaction and a globular

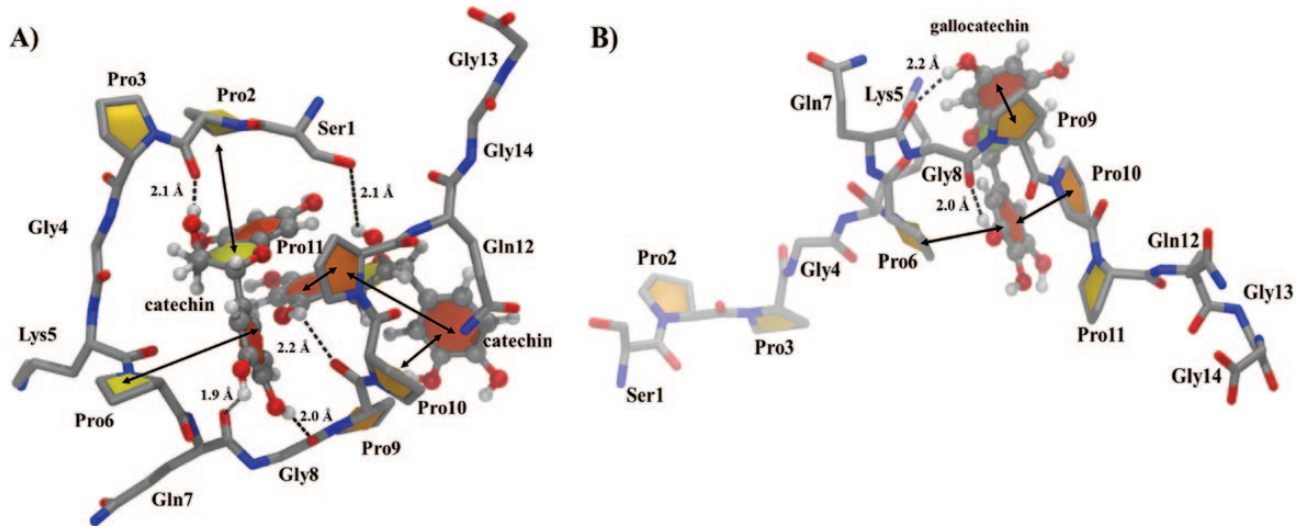

Figure 2. Representation of the geometries of $IB7_{14}$:$(CAT)_2$ (**A**) and ($IB7_{14}$):$(GAL)_1$ (**B**) after 40 ns of MD simulation. The $IB7_{14}$ peptide and polyphenol molecules are depicted with sticks and vdW (respectively) and are colored by atom type.

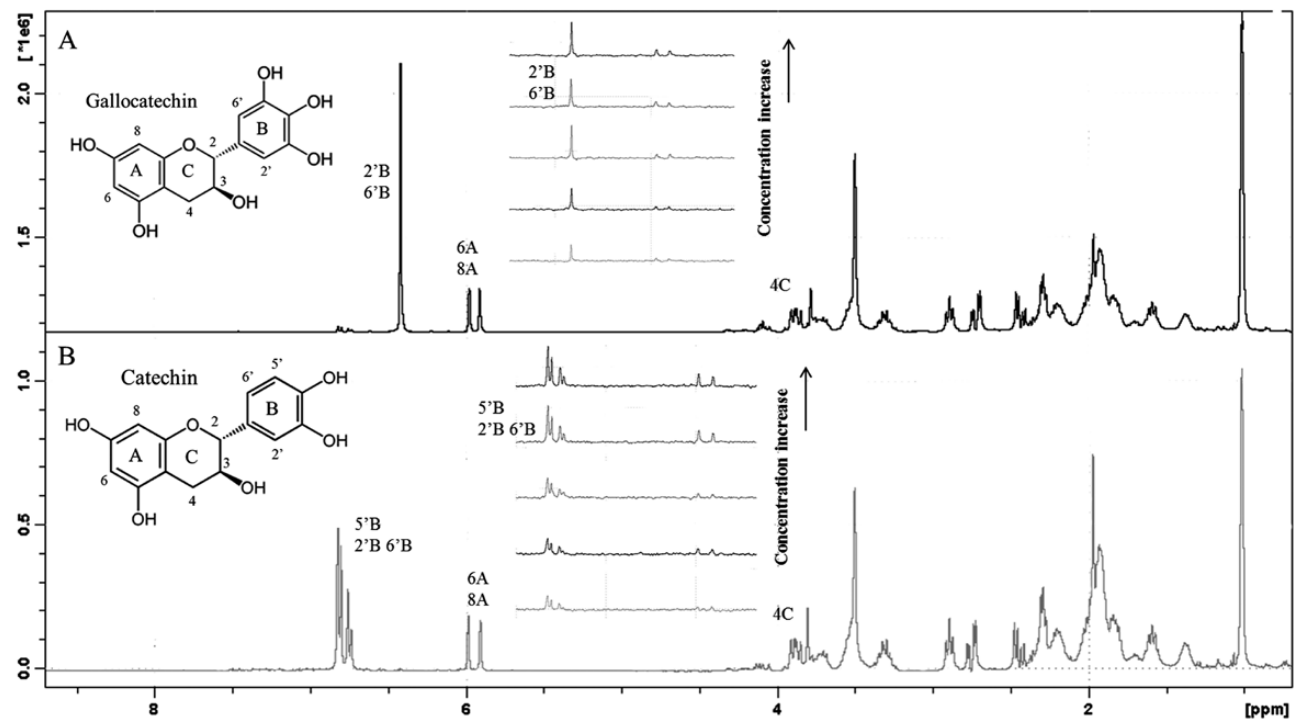

Figure 3. STD NMR spectra of the mixture of GAL (**A**) and CAT (**B**) with the peptide $IB7_{12}$.

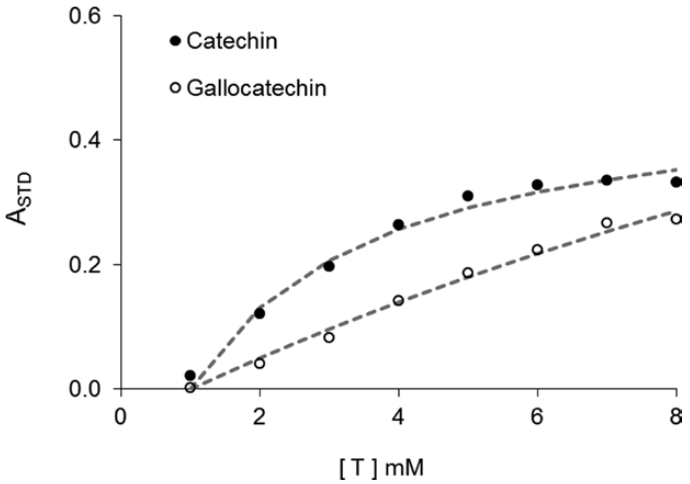

Figure 4. Observed (symbols) and fitted (line) STD amplification factor according to eq. 2.

conformation for CAT-peptide interaction, which may reinforce the affinity between the flavanol and the peptide.

The solvent-accessible surface area (SASA) values were determined for the peptide residues during each MD simulation. These values evaluate the surface area of the $IB7_{14}$ fragment that is accessible to a solvent probe, which could indicate the extension of polyphenols' binding. It was observed that the SASA value of the peptide decreases much faster in the presence of CAT molecules than in the presence of GAL molecules, which suggest a larger binding extension of the former compound. For example, in the $IB7_{14}$:$(CAT)_8$ system (MD-1 simulation), the SASA value rapidly decreased from 1710.6 ± 84.8 Å^2 (first 5 ns) to 1497.0 ± 130.3 Å^2 (between 15 and 25 ns), and finally to 1418.4 ± 70.4 Å^2 in the last 5 ns of simulation. This translates into a maximum decrease of 17.1%. However, in a model system with gallocatechin molecules (MD-1 simulation), the initial SASA value only decreases to 1692.9 ± 96.0 Å^2 (maximum value of 1%). Overall, all these computational data suggest that the extension of polyphenols binding to the $IB7_{14}$ peptide is the following: CAT > GAL, which is in agreement with the experimental studies performed and may justify the higher astringent ability of the former compound.

STD NMR experiments

In order to quantify the strength of the interactions, the binding affinity between both gallocatechin and CAT toward IB7 was followed by measuring the intensities of protons (2′B, 5′B and 6B). Figure 3 shows the STD NMR spectra of the mixture of gallocatechin and CAT with the peptide $IB7_{12}$. Differences between *off-resonance* and *on-resonance* spectra (eq. 1), with increasing tannin concentration, were used to calculate the amplification factor and the dissociation constant (eq. 2).

Figure 4 shows the observed (symbols) and fitted (lines) amplification factor (A_{STD}) of gallocatechin and CAT, at increasing concentrations. The behavior observed in the plot for each compound indicates differences in the occupation of the receptor-binding sites (Viegas et al. 2011). According to the obtained dissociation constants, the affinity of CAT (K_D = 2.7 mM) was higher than GAL (K_D = 25.7 mM). Dissociation constants ranging from 0.4 to 8 mM have been shown by Cala et al. (2010, 2012) for the interactions between the peptides $IB7_{14}$ and $IB9_{37}$ and procyanidins dimers and trimers. Results show the importance of the hydroxylation B-ring flavanols in the interaction with salivary proteins, which, on one hand, corroborates results generated in silico and, on the other hand, demonstrates that $IB7_{12}$ retains the behavior expected for $IB7_{14}$.

Conclusions

Real and theoretical experiments have been carried out in order to better explain the molecular mechanisms responsible for the sensations elicited by flavanols in mouth. Flavanols studied have been trihydroxylated B-ring (GAL and GAL-derivatives) and dihydroxylated B-ring flavanols (CAT and CAT-derivatives). Most of studies devoted to flavanols astringency have been carried out in vitro models and a real relationship with what is occurring in the oral cavity is avoided. In this work, we have studied sensations elicited by flavanols by means of a sensory panel and to obtain further insights into the mechanisms of action we have turn to molecular dynamic simulations and STD NMR experiments. Results obtained from sensory analysis show clear differences in bitterness, intensity of astringency and astringency qualities between the 2 types of flavanols tested. In general, dihydroxylated B-ring flavanols were more astringent, bitter, dry, rough, unripe, and persistent than trihydroxylated B-ring flavanols. Besides, these last compounds were smoother, more velvety, and viscous. Hence, pleasant oral sensations seemed to be more related to GAL and prodelphinidins, whereas CAT and procyanidins reached higher scores in the unpleasant ones.

MD simulations suggested that CAT binds to $IB7_{14}$ faster than GAL and this interaction is maintained for more time. $IB7_{14}$ can interact with 2 CAT molecules concurrently while only interacts with 1 GAL molecule. The decrease observed in the SASA value when binding CAT suggests a larger binding extension for this compound compared with GAL.

MD simulations and STD NMR experiments support the results obtained from the tasting panel, which revealed CAT as more astringent and persistent than GAL. The differences observed between the 2 monomers indicate that the number of hydroxyl substituents present in B-ring of the flavanic nucleus is decisive for the interaction with salivary proteins and the development of astringency perception, and nicely outline the interest of the study of the interactions of prodelphinidins and salivary proteins.

Funding

The work was supported by Spanish MICINN (Projects ref. AGL2011-30254-C02-01 and AGL2014-58486-C2-1-R) and Fundação para a Ciência e Tecnologia (ref. IF/01355/2014 and NORTE-07-0162-FEDER-000048).

Acknowledgments

The authors also thank the panellists, particularly Dra. Álvarez-Cano, for their contribution. R. Ferrer-Gallego thanks Fundación Alfonso Martín Escudero for the post-doctoral fellowship and N. Quijada-Morín also thanks the Spanish MICINN for the F.P.I. predoctoral scholarship.

References

Bayly CI, Cieplak P, Cornell WD, Kollman PA. 1993. A well-behaved electrostatic potential based method using charge restraints for deriving atomic charges—the Resp Model. *J Phys Chem*. 97: 10269–10280.

Cala O, Pinaud N, Simon C, Fouquet E, Laguerre M, Dufourc EJ, Pianet I. 2010. NMR and molecular modeling of wine tannins binding to saliva proteins: revisiting astringency from molecular and colloidal prospects. *FASEB J*. 24(11):4281–4290.

Cala O, Dufourc EJ, Fouquet E, Manigand C, Laguerre M, Pianet I. 2012. The colloidal state of tannins impacts the nature of their interaction with proteins: the case of salivary proline-rich protein/procyanidins binding. *Langmuir*. 28(50):17410–17418.

Cala O, Fabre S, Pinaud N, Dufourc EJ, Fouquet E, Laguerre M, Pianet I. 2011. Towards a molecular interpretation of astringency: synthesis, 3D structure, colloidal state, and human saliva protein recognition of procyanidins. *Planta Med*. 77(11):1116–1122.

Case DA, Darden TA, Cheatham TEI, Simmerling CL, Wang J, Duke RE, Luo R, Walker RC, Zhang W, Merz KM, *et al*. 2012. *AMBER 12*. San Francisco (CA): University of California.

Collins JM, Leadbeater NE. 2007. Microwave energy: a versatile tool for the biosciences. *Org Biomol Chem*. 5(8):1141–1150.

Cornell WD, Cieplak P, Bayly CI, Gould IR, Merz KM, Ferguson DM, Spellmeyer DC, Fox T, Caldwell JW, Kollman PA. 1995. A 2nd generation force-field for the simulation of proteins, nucleic-acids, and organic-molecules. *J Am Chem Soc*. 117:5179–5197.

de Freitas V, Carvalho E, Mateus N. 2003. Study of carbohydrate influence on protein-tannin aggregation by nephelometry. *Food Chem*. 81:503–509.

de Freitas V, Mateus N. 2012. Protein/polyphenol interactions: past and present contributions. Mechanisms of astringency perception. *Curr Org Chem*. 16:724–746.

Essmann U, Perera L, Berkowitz ML, Darden T, Lee H, Pedersen LG. 1995. A smooth particle mesh Ewald method. *J Chem Phys*. 103:8577–8593.

Fernandes A, Brás NF, Mateus N, de Freitas V. 2014. Understanding the molecular mechanism of anthocyanin binding to pectin. *Langmuir*. 30(28):8516–8527.

Ferrer-Gallego R, García-Marino M, Hernández-Hierro JM, Rivas-Gonzalo JC, Escribano-Bailón MT. 2010. Statistical correlation between flavanolic composition, colour and sensorial parameters in grape seed during ripening. *Anal Chim Acta*. 660(1–2):22–28.

Ferrer-Gallego R, Gonçalves R, Rivas-Gonzalo JC, Escribano-Bailón MT, de Freitas V. 2012a. Interaction of phenolic compounds with bovine serum albumin (BSA) and α-amylase and their relationship to astringency perception. *Food Chem*. 135(2):651–658.

Ferrer-Gallego R, Hernández-Hierro JM, Rivas-Gonzalo JC, Escribano-Bailón MT. 2012b. Influence of climatic conditions on the phenolic composition of Vitis vinifera L. cv. Graciano. *Anal Chim Acta*. 732:73–77.

Ferrer-Gallego R, Hernández-Hierro JM, Rivas-Gonzalo JC, Escribano-Bailón MT. 2014. Sensory evaluation of bitterness and astringency sub-qualities of wine phenolic compounds: synergistic effect and modulation by aromas. *Food Res Int*. 62:1100–1107.

Fields GB, Noble RL. 1990. Solid phase peptide synthesis utilizing 9-fluorenylmethoxycarbonyl amino acids. *Int J Pept Protein Res*. 35(3):161–214.

Frisch MJ, Trucks GW, Schlegel HB, Scuseria GE, Robb MA, Cheeseman JR, Scalmani G, Barone V, Mennucci B, Petersson GA, *et al*. 2009. *Gaussian 09*. Wallingford (CT): Gaussian, Inc.

Gawel R, Iland PG, Francis IL. 2001. Characterizing the astringency of red wine: a case study. *Food Qual Prefer*. 12:83–94.

Gibbins HL, Carpenter GH. 2013. Alternative mechanisms of astringency—what is the role of saliva? *J Texture Stud*. 44:364–375.

Gil M, Kontoudakis N, González E, Esteruelas M, Fort F, Canals JM, Zamora F. 2012. Influence of grape maturity and maceration length on color, polyphenolic composition, and polysaccharide content of Cabernet Sauvignon and Tempranillo wines. *J Agric Food Chem*. 60(32):7988–8001.

Green BG, Dalton P, Cowart B, Shaffer G, Rankin K, Higgins J. 1996. Evaluating the 'Labeled Magnitude Scale' for measuring sensations of taste and smell. *Chem Senses*. 21(3):323–334.

Gonçalves R, Mateus N, Pianet I, Laguerre M, de Freitas V. 2011. Mechanisms of tannin-induced trypsin inhibition: a molecular approach. *Langmuir*. 27(21):13122–13129.

Fields GB. 1997. Trifluoroacetic acid cleavage and deprotection of resin-bound peptides following synthesis by Fmoc chemistry. *Methods Enzymol*. 289:67–83.

Izaguirre JA, Catarello DP, Wozniak JM, Skeel RD. 2001. Langevin stabilization of molecular dynamics. *J Chem Phys*. 114: 2090–2098.

Jöbstl E, O'Connell J, Fairclough JP, Williamson MP. 2004. Molecular model for astringency produced by polyphenol/protein interactions. *Biomacromolecules*. 5(3):942–949.

Kallithraka S, Bakker J, Clifford MN. 1997. Evaluation of bitterness and astringency of (+)-catechin and (−)-epicatechin in red wine and in model solution. *J Sens Stud*. 12:25–37.

Kennedy JA, Jones GP. 2001. Analysis of proanthocyanidin cleavage products following acid-catalysis in the presence of excess phloroglucinol. *J Agric Food Chem*. 49(4):1740–1746.

Kurogi M, Miyashita M, Emoto Y, Kubo Y, Saitoh O. 2012. Green tea polyphenol epigallocatechin gallate activates TRPA1 in an intestinal enteroendocrine cell line, STC-1. *Chem Senses*. 37(2):167–177.

Lee CA, Ismail B, Vickers ZM. 2012. The role of salivary proteins in the mechanism of astringency. *J Food Sci*. 77(4):C381–C387.

Lee CB, Lawless HT. 1991. Time-course of astringent sensations. *Chem Senses*. 16:225–238.

Madigan D, McMurrough I, Smyth MR. 1994. Determination of proanthocyanidins and catechins in beer and barley by high-performance liquid chromatography with dual-electrode electrochemical detection. *Analyst*. 119(5):863–868.

McRae JM, Schulkin A, Kassara S, Holt HE, Smith PA. 2013. Sensory properties of wine tannin fractions: implications for in-mouth sensory properties. *J Agric Food Chem*. 61(3):719–727.

Quijada-Morín N, Regueiro J, Simal-Gándara J, Tomás E, Rivas-Gonzalo JC, Escribano-Bailón MT. 2012. Relationship between the sensory-determined astringency and the flavanolic composition of red wines. *J Agric Food Chem*. 60(50):12355–12361.

Robichaud JL, Noble AC. 1990. Astringency and bitterness of selected phenolics in wine. *J Sci Food Agric*. 53:343–353.

Rossetti D, Bongaerts JHH, Wantling E, Stokes JR, Williamson AM. 2009. Astringency of tea catechins: more than an oral lubrication tactile percept. *Food Hydrocolloid*. 23:1984–1992.

Ryckaert JP, Ciccotti G, Berendsen HJC. 1977. Numerical-integration of Cartesian equations of motion of a system with constraints—molecular-dynamics of N-alkanes. *J Comput Phys*. 23:327–341.

Schwarz B, Hofmann T. 2008. Is there a direct relationship between oral astringency and human salivary protein binding? *Eur Food Res Technol*. 227:1693–1698.

Scollary GR, Pasti G, Kallay M, Blackman J, Clark AC. 2012. Astringency response of red wines: potential role of molecular assembly. *Trends Food Sci Technol*. 27:25–36.

Simon C, Barathieu K, Laguerre M, Schmitter JM, Fouquet E, Pianet I, Dufourc EJ. 2003. Three-dimensional structure and dynamics of wine tannin-saliva protein complexes. A multitechnique approach. *Biochemistry*. 42(35):10385–10395.

Soares S, Sousa A, Mateus N, de Freitas V. 2012. Effect of condensed tannins addition on the astringency of red wines. *Chem Senses*. 37(2):191–198.

Sun B, de Sá M, Leandro C, Caldeira I, Duarte FL, Spranger I. 2013. Reactivity of polymeric proanthocyanidins toward salivary proteins and their contribution to young red wine astringency. *J Agric Food Chem*. 61(4):939–946.

Thorngate JH, Noble AC. 1995. Sensory evaluation of bitterness and astringency of 3R(−)-epicatechin and 3S(+)-catechin. *J Sci Food Agric*. 67:531–535.

Viegas A, Manso J, Nobrega FL, Cabrita EJ. 2011. Saturation-transfer difference (STD) NMR: a simple and fast method for ligand screening and characterization of protein binding. *J. Chem. Educ*. 88:990–994.

Wang J, Wolf RM, Caldwell JW, Kollman PA, Case DA. 2004. Development and testing of a general amber force field. *J Comput Chem*. 25(9):1157–1174.

Wollmann N, Hofmann T. 2013. Compositional and sensory characterization of red wine polymers. *J Agric Food Chem*. 61(9):2045–2061.